ACS Sustainable Chemistry & Engineering

Research Article

pubs.acs.org/journal/ascecg

Mesoporous Nickel Ferrites with Spinel Structure Prepared by an Aerosol Spray Pyrolysis Method for Photocatalytic Hydrogen Evolution

Dachao Hong,[†] Yusuke Yamada,[†] Margaret Sheehan,[‡] Shinya Shikano,[†] Chun-Hong Kuo,[‡] Ming Tian,[‡] Chia-Kuang Tsung,*[,‡] and Shunichi Fukuzumi*[,†]

[†]Department of Material and Life Science, Graduate School of Engineering, ALCA, Japan Science and Technology Agency, Osaka University, Suita, Osaka 565-0871, Japan

[‡]Department of Chemistry, Merkert Chemistry Center, Boston College, 2609 Beacon Street, Chestnut Hill, Massachusetts 02467, United States

Supporting Information

ABSTRACT: Submicron-sized mesoporous nickel ferrite ($NiFe_2O_4$) spheres were prepared by an aerosol spray pyrolysis method using Pluronic F127 as a structure-directing agent, and their photocatalytic performance for hydrogen (H_2) evolution was examined in an aqueous MeOH solution by visible light irradiation (λ > 420 nm). The structure of the spherical mesoporous nickel ferrites was studied by transmission electron microscopy, powder X-ray diffraction, and N_2 adsorption−desorption isotherm measurements. Mesoporous $NiFe_2O_4$ spheres of high specific surface area (278 m^2 g^{-1}) with a highly crystalline framework were prepared by adjusting the amount of structure-directing agent and the calcining condition. High photocatalytic activity of mesoporous $NiFe_2O_4$ for H_2 evolution from water with methanol was achieved due to the combination of high surface area and high crystallinity of the nickel ferrites.

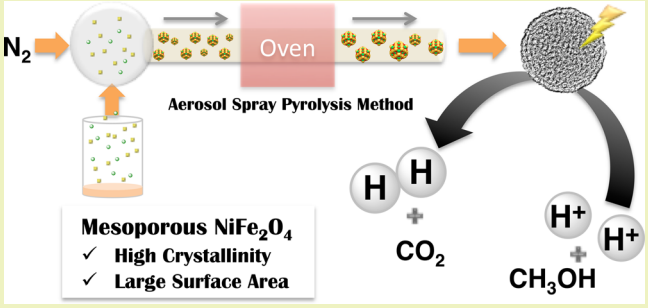

KEYWORDS: *Nickel ferrite, Hydrogen evolution, Photocatalysis, Metal oxide sphere, Crystallinilty, Surface area, Ramp rate*

INTRODUCTION

Metal oxides are of great interest for a variety of applications due to their unique catalytic, photocatalytic, electronic, and optical properties.[1,2] Chemical composition, crystallinity, and surface area are all primary determinants for the performance of metal oxides in catalysis and photocatalysis.[3,4] In particular, multicomponent metal oxides with high surface area could have great catalytic performance due to the synergetic composite effect attributed to the multicomponent structure and the larger number of active sites available through the high surface area.[5−8] Spinel nickel ferrite ($NiFe_2O_4$), a multicomponent metal oxide composed of only earth-abundant metals, is an attractive material due to its promising catalytic applications in various reactions such as sulfuric acid decomposition,[9,10] selective oxidation of CO,[11] thermochemical water splitting,[12−14] and electrocatalytic hydrogen (H_2) evolution.[15] Recently, photocatalytic H_2 evolution utilizing solar energy has attracted much attention for realizing an energy sustainable society.[16−22] Nickel ferrite has been reported to exhibit photocatalytic activity for visible light-driven H_2 evolution[23,24] and water oxidation.[25] In addition, the ferromagnetic properties of nickel ferrite have allowed the easy separation of its particles from a reaction solution.[25]

Nickel ferrite has been prepared by several different methods for morphological control.[26−32] For example, a hydrothermal method in a basic solution was reported to prepare micron-sized octahedral nickel ferrite crystals.[28] Nickel ferrite nanoparticles with a size of 7.1 nm were prepared by a solvothermal method in hexanol.[29] Sol−gel combustion can also produce nano-sized nickel ferrites by using citric acid as a capping agent.[30] Monodispersed nickel ferrite was reported to be prepared by sol−gel coprecipitation of nickel and iron chloride in ethylene glycol.[31] To increase the surface area for catalysis applications, Shi et al. have demonstrated the first mesoporous nickel ferrite synthesis by calcining $NiFe_2(C_2O_4)_3$ as a precursor.[32] In their work, the surface area of nickel ferrite reached 302 m^2 g^{-1} with relatively low crystallinity. The crystallinity was increased by calcining the material at 700 °C; however, the surface area decreased to 63 m^2 g^{-1}. These pioneer works have demonstrated the great potential of nickel ferrites; therefore, a method for synthesizing nickel ferrite with both high surface area and high crystallinity is strongly desired for applications in catalysis. The aerosol spray pyrolysis method

Received: July 26, 2014
Revised: September 20, 2014
Published: October 6, 2014

is a promising strategy for increasing both surface area and crystallinity, enabling sequential, easy, and large-scale production of metal oxide spheres.[33−39] However, mesoporous nickel ferrites have yet to be prepared by an aerosol spray pyrolysis method for photocatalytic H_2 evolution.

Herein, we report the synthesis of spherical mesoporous nickel ferrite, $NiFe_2O_4$, by a self-assembly associated aerosol spray pyrolysis method[35] and the study of their photocatalytic performance in H_2 evolution from water with methanol. In this process, Pluronic F127 was used as an amphiphilic organic structure-directing agent, and nickel nitrate and iron nitrate were used as inorganic precursors for the oxide. Self-assembly of organic and inorganic species followed by metal nitrate decomposition and inorganic polymerization were accomplished in the ethanol aerosol droplets in N_2 atmosphere at 400 °C. Mesoporous crystalline nickel ferrite spheres were obtained after the spheres were calcined at 300 °C in air to remove the structure-directing agent and increase crystallinity. The concentrations of the structure-directing agent were varied to tune the surface areas and pore sizes of the mesoporous nickel ferrites. The obtained mesoporous nickel ferrites were characterized by powder X-ray diffraction (XRD), transmission electron microscopy (TEM), N_2 sorption, and thermogravimetric/differential thermal analysis (TG/DTA).

Mesoporous nickel ferrites were used as visible light photocatalysts for H_2 evolution due to their narrow band gap energy (about 1.7 eV) capable of absorbing visible light, as well as the conduction band edge [about −0.6 V vs normal H_2 electrode (NHE)], which is negative enough to reduce protons to generate H_2.[23] H_2 was evolved by photoirradiation (λ > 420 nm) from an aqueous suspension containing spherical mesoporous nickel ferrites and methanol, which act as a photocatalyst and a sacrificial electron donor, respectively. High photocatalytic activity resulted from both high crystallinity and high surface area of the spherical mesoporous nickel ferrites.

EXPERIMENTAL SECTION

Materials. All chemicals used for synthesis were obtained from chemical companies and used without further purification. Nickel(II) nitrate hexahydrate, iron(III) nitrate hexahydrate, and Pluronic F127 were purchased from Sigma-Aldrich Co. Purified water was provided by a Millipore Milli-Q water purification system (18.2 MΩ cm).

Synthesis of Spherical Mesoporous Nickel Ferrites. A certain amount of surfactant Pluronic F127 (0.75 or 1.50 g) was dissolved in 150 mL of ethanol and sonicated until it formed a clear solution. Nickel(II) nitrate hexahydrate (0.66 mmol) and iron(III) nitrate hexahydrate (1.33 mmol) were added into the solution with vigorous stirring. The solution was used as a precursor for the aerosol spray process (Figure S1, Supporting Information). During the aerosol spray process, the solvent in the aerosol droplets was evaporated, and the organic and inorganic species were assembled at 50 °C in the assembly chamber before passing through the heating zone set at 400 °C. The resultant powder product was collected on a filter paper with a mesh size of 220 nm. The reactor was operated at a volumetric flow rate of 5 L (STP) min^{-1}. These as-synthesized mesostructured organic−inorganic hybrid spheres were then calcined at 300 °C (ramp rate: 1 °C min^{-1} or 5 °C min^{-1}) in air for 5 h to obtain mesoporous nickel ferrite spheres.

Synthesis of Reference $NiFe_2O_4$.[23] An aqueous solution (6.0 mL) containing $Na_2C_2O_4$ (48 mmol) was added to an aqueous solution (60 mL) containing nickel(II) nitrate hexahydrate (24 mmol), iron(II) sulfate heptahydrate (48 mmol), and Pluronic F127 (2.0 g) with magnetic stirring at room temperature (RT). After stirring for 20 min, the resulting mixture was hydrothermally treated at 100 °C for 30 h in an autoclave of 140 mL capacity. The precursor was collected by centrifugation, washed with water and ethanol several times, and then calcined at 500 °C for 2 h with a ramp rate of 5 °C min^{-1} to obtain $NiFe_2O_4$.

Characterization. TEM images of nanoparticles, which were mounted on a copper microgrid coated with elastic carbon, were obtained on a JEOL JEM2010F operated at 200 kV. X-ray diffraction patterns were recorded by a Rigaku MiniFlex 600. Incident X-ray radiation was produced by a Cu X-ray tube, operating at 40 kV and 15 mA with Cu Kα radiation of 1.54 Å. The scanning rate was 2° min^{-1} from 20° to 70° in 2θ. Nitrogen adsorption−desorption at −196 °C was performed with a Belsorp-mini (BEL Japan, Inc.) within a relative pressure range from 0.01 to 101.3 kPa. A sample mass of ∼80 mg was used for adsorption analysis after pretreatment at 120 °C for ∼1.0 h under vacuum conditions and kept in N_2 atmosphere until N_2 adsorption−desorption measurements. The sample was exposed to a mixed gas of He and N_2 with a programmed ratio, and the adsorbed amount of N_2 was calculated from the change in pressure within a cell after reaching equilibrium (at least 5 min). The diffuse reflectance spectra were recorded with a V-670 spectrophotometer (JASCO). TG/DTA data were recorded on an SII TG/DTA 7200 instrument. Each sample (∼5.0 mg) was heated from 20 to 600 °C with a ramp rate of 1 or 5 °C min^{-1}. A certain amount of α-Al_2O_3 was used as a reference for DTA measurements.

Photocatalytic H_2 Evolution. A pretreatment to remove carbonaceous residues in the mesoporous nickel ferrite photocatalysts was performed as follows. An aqueous suspension (5.0 mL) containing a nickel ferrite photocatalyst (2.0 mg) in a Schlenk flask (19.0 mL) sealed with a rubber septum was irradiated with a xenon lamp (Ushio Optical, Model X SX-UID 500X AMQ) through a color filter glass (Asahi Techno Glass) transmitting λ > 420 nm at room temperature. After the pretreatment, the photocatalyst was collected by centrifugation and used for the H_2-evolution reaction. The photocatalytic H_2 evolution was started by photoirradiation (λ > 420 nm) of a mixed suspension of H_2O (4.0 mL) and methanol (1.0 mL) with the collected photocatalyst in the Schlenk flask. A small portion (100 μL) of the gas in the headspace of the Schlenk flask was sampled by a gastight syringe and used for gas chromatography (GC) analysis [Shimadzu GC-14B gas chromatograph (N_2 carrier, active carbon with a particle size of 60−80 mesh at 80 °C) equipped with a thermal conductivity detector].

For action spectra, a square quartz cuvette filled with a mixed suspension of H_2O (2.0 mL) and methanol (0.5 mL) containing nickel ferrite (1.0 mg) was irradiated by monochromatized light of λ = 500, 650, and 700 nm from a Shimadzu RF-5300PC fluorescence spectrometer after the pretreatment. A detailed determination method of an apparent quantum yield is described in the Supporting Information.

RESULTS AND DISCUSSION

Precursors of Nickel Ferrite. In the self-assembly associated aerosol spray process, the aerosol droplets containing the structure-directing agent, nickel nitrate, and iron nitrate were generated by an ultrasonic humidifier. The droplets were carried by N_2 through a spherical quartz chamber heated at 50 °C prior to the main heating zone heated at 400 °C. The solvent evaporation at 50 °C in the chamber induced the self-assembly between the structure-directing agent and the metal ions.[38] The decomposition and condensation of the metal precursors occurred through the main heating zone (400 °C). TEM images of the products exhibited sphere topology as shown in Figure S2 of the Supporting Information. The collected powder product was calcined at 300 °C for 5 h in air to remove the structure-directing agent and to increase the crystallinity of the inorganic frameworks of the nickel ferrites.

Characterization of Mesoporous Nickel Ferrite Spheres. Nickel ferrite spheres denoted as **NF5** and **NF10a** were prepared by the aerosol spray process using different concentrations of the structure-directing agent (5 g L^{-1} and 10

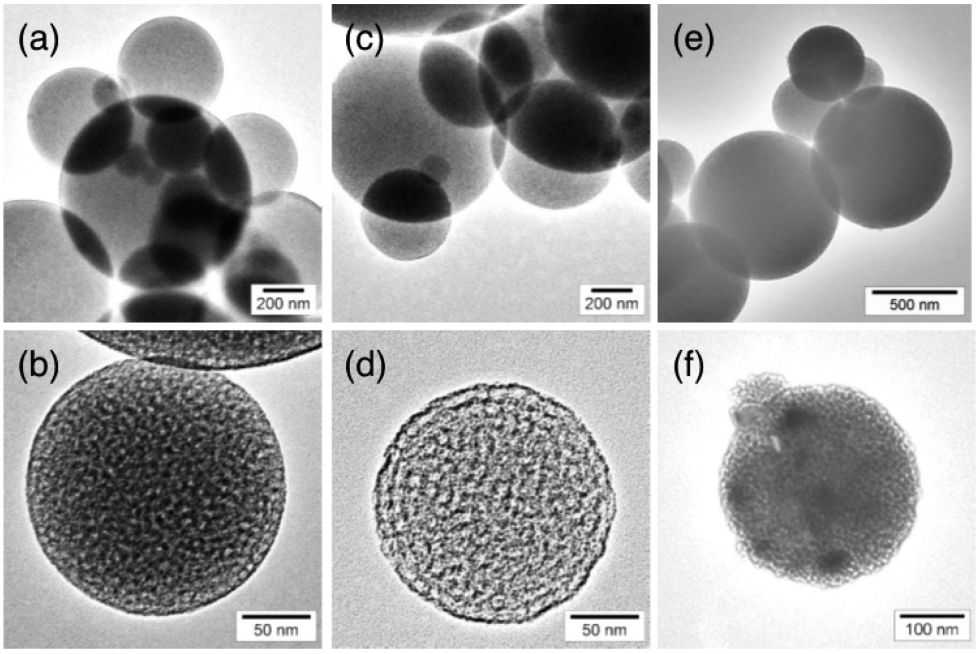

Figure 1. TEM images of mesoporous nickel ferrites: (a, b) **NF5**, (c, d) **NF10a**, and (e, f) **NF10b**.

g L^{-1}, respectively) and then were calcined at 300 °C with a ramp rate of 1 °C min^{-1}. The spherical and porous structures of the nickel ferrites were confirmed by TEM as shown in Figure 1. The size of the mesoporous nickel ferrite spheres is random, around a few hundred nanometers. As the concentration of the structure-directing agent increases, the observed pore size becomes larger as shown in Figure 1b and d. The pore density also increases, which is further confirmed by N_2 adsorption–desorption as discussed later. This higher porosity could benefit the catalytic applications. SEM-EDX measurements were also performed with the mesoporous nickel ferrites (Figure S3, Supporting Information). The EDX results demonstrate that the mesoporous nickel ferrite spheres are composed of Ni and Fe with the 1:2 atomic ratio.

The crystal structure of **NF10a** was characterized by powder XRD as shown in Figure 2. **NF10a** is nearly amorphous (**NF5a** is nearly amorphous as well), although several broad diffraction peaks are identified as (3 1 1), (4 0 0), and (4 4 0) reflections. In order to increase the crystallinity of **NF10a**, which has a higher degree of porosity, we have tuned calcination conditions. The spheres labeled as **NF10b** were prepared in the same manner as **NF10a** except that the materials were calcined to 300 °C with a ramp rate of 5 °C min^{-1}. To our surprise, when the ramp rate was increased to 5 °C min^{-1}, the crystallinity of the spinel structure was indeed enhanced. The XRD pattern was consistent with the previous reports.[23−25] The difference in crystallinity depending on the ramp rate could be ascribed to the combustion of the organic structure-directing agents in **NF10a** and **NF10b**. The different combustion behaviors were revealed by TG/DTA study (Figure 3). The higher ramp rate induced ignition of the structure-directing agent, and the spheres burst into flame. This sharp temperature increase improved the crystallinity.[33] This result demonstrates that the crystallinity of nickel ferrites can be improved by increasing the ramp rate instead of increasing calcination temperature and time, which could damage the mesostructure of the materials. TEM images of **NF10b** observed in Figure 1e and f indicate that the mesostructure of the spheres was maintained with the higher crystallinity.

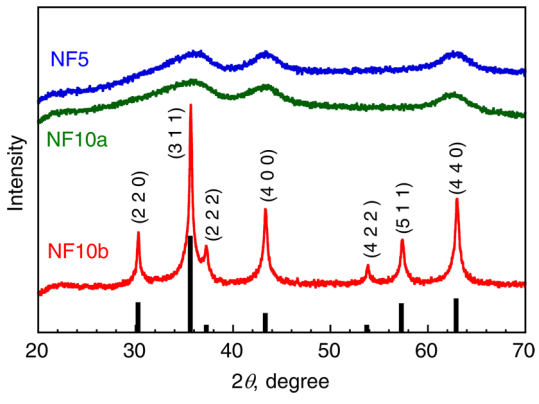

Figure 2. Powder XRD patterns of mesoporous nickel ferrites prepared with different concentrations of structure-directing agent Pluronic F127 (**NF5**, 5 g L^{-1} and **NF10a**, 10 g L^{-1}). The samples were calcined with a ramp rate of 1 °C min^{-1}. **NF10b** was prepared with the concentration of 10 g L^{-1} of Pluronic F127 and calcined with a ramp rate of 5 °C min^{-1}. The black bars indicate the XRD peak positions of $NiFe_2O_4$ reported in the literature.[28]

The mesoporous structure of nickel ferrites was further studied by N_2 adsorption–desorption measurements. Figure 4 shows the N_2 adsorption–desorption isotherms of the mesoporous nickel ferrites and the Barrett–Joyner–Halenda (BJH) plots obtained from N_2-adsorption measurements at −196 °C. The Brunauer–Emmett–Teller (BET) surface areas and the BJH pore sizes and volumes of the mesoporous nickel ferrites are summarized in Table 1, along with those of reference $NiFe_2O_4$ prepared by a literature method.[23] Reference $NiFe_2O_4$ was characterized by powder XRD, SEM, and EDX spectra (Figures S4, S5, and S6, respectively, Supporting Information), although reference $NiFe_2O_4$ contains a small amount of Fe_2O_3, which has little effect on the photocatalytic H_2 evolution due to its highly positive conduction band edge.[21] The isotherm features of the mesoporous nickel ferrites can be

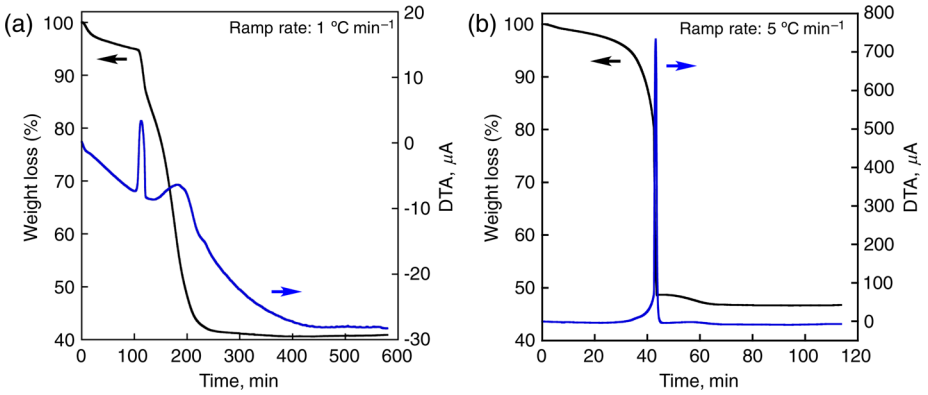

Figure 3. TG/DTA for the precursors of **NF10a** and **NF10b**. The temperature increased from 20 to 600 °C with a ramp rate of (a) 1 °C min^{-1} and (b) 5 °C min^{-1}.

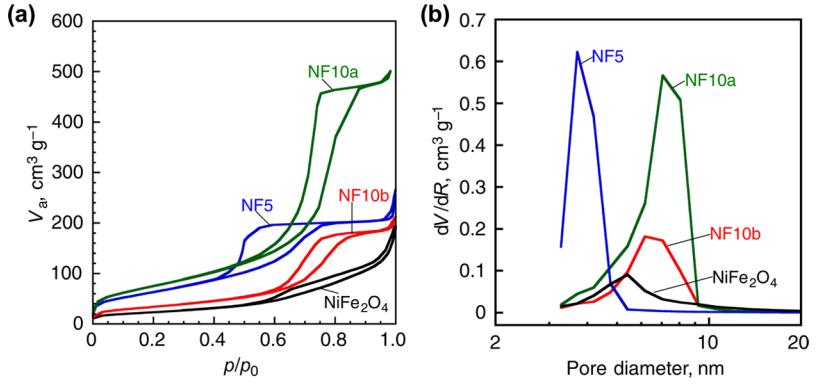

Figure 4. (a) N_2 adsorption−desorption isotherms and (d) BJH plots of mesoporous nickel ferrites mesoporous nickel ferrites; **NF5** (blue), **NF10a** (green), **NF10b** (red), and reference $NiFe_2O_4$ (black).

Table 1. Crystallinity, BET Surface Areas, BJH Pore Size, Volumes, and H_2-Evolution Rates Observed with Mesoporous Nickel Ferrites and Reference $NiFe_2O_4$

sample	crystallinity	BET surface area (m^2 g^{-1})	d_{BJH} (nm)	V_{BJH} (cm^3 g^{-1})	R_{H2}[a] (μmol h^{-1})
NF5	amorphous	235	3.7	0.38	0.02
NF10a	amorphous	278	7.1	0.84	0.02
NF10b	spinel	121	6.2	0.33	0.09
$NiFe_2O_4$[b]	spinel	81	5.4	0.29	0.03

[a] H_2 evolution was observed after 5 h of photoirradiation (λ > 420 nm) of a reaction suspension [methanol/water, 1/4 (v/v)] containing a photocatalyst (2.0 mg). [b] In a previous study, a high H_2 evolution rate of 2.78 μmol h^{-1} was reported for the photocatalytic system under photoirradiation (λ > 420 nm) of a mixed solution of H_2O and MeOH [100 mL, 1:4 (v/v)] containing a large amount of $NiFe_2O_4$ (100 mg).[23]

assigned to type IV, having a hysteresis loop.[40] The isotherms with hysteresis loops demonstrate the mesoporous structure in the nickel ferrites. The type of hysteresis loops of **NF5**, **NF10a**, and **NF10b** were classified as an H2 feature according to classification of adsorption hysteresis.[40] **NF10a** exhibits higher surface area and pore size (278 m^2 g^{-1}, 7.1 nm) than those of **NF5** (235 m^2 g^{-1}, 3.7 nm), which is in agreement with the TEM observation. Although the surface area of **NF10b** (121 m^2 g^{-1}) is lower than that of **NF10a** due to its higher crystallinity, it is still higher than that observed for reference $NiFe_2O_4$ (81 m^2 g^{-1}), which was prepared by the sol−gel combustion method. The reference $NiFe_2O_4$ also exhibited a hysteresis loop in the isotherm with an H3 feature, which is ascribed to the agglomeration of particles.

The diffuse reflectance UV−vis spectra (DRS) of the mesoporous nickel ferrites are shown in Figure 5, which

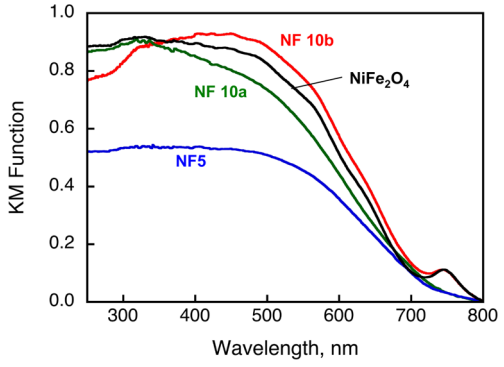

Figure 5. Diffuse reflectance UV−vis spectra of mesoporous nickel ferrites (**NF5**, **NF10a**, and **NF10b**) and reference $NiFe_2O_4$.

confirms that the synthesized nickel ferrites have an absorption in the visible region. **NF10b** and reference $NiFe_2O_4$ prepared by sol−gel combustion show a characteristic absorption band around 746 nm due to the crystalline spinel structure. On the other hand, amorphous spheres of **NF5** and **NF10a** exhibited no shoulder peak around 746 nm. These results are consistent with previous reports.[23] The absorption bands of the nickel ferrites suggest that their band gaps are estimated to be around 1.7 eV by considering the similarity of the absorption band

dx.doi.org/10.1021/sc500484b | ACS Sustainable Chem. Eng. 2014, 2, 2588−2594

reported in the literature.[23,41] In general, a valence band of a metal oxide semiconductor is mainly composed of O 2p orbitals, in which the valence band maximum (VBM) locates at more positive potential than 3.0 V vs NHE. However, a theoretical study of the electronic structure and band gap of $NiFe_2O_4$ suggests that the VBM of $NiFe_2O_4$ mainly composed of both Ni and O orbitals shifts to a negative potential by about 2 eV.[41,42] Also, the different localization of the VBM (mostly on Ni and O) and the conduction band minimum (mostly on Fe and O) resulted in well-separated electron−hole pairs generated by photoabsorption.[41] Thus, the mesoporous nickel ferrites were used as visible light-driven photocatalysts for H_2 evolution to investigate the relationship between the catalytic performance and structure.

Activity for Photocatalytic H_2 Evolution. The well-characterized mesoporous nickel ferrites acted as photocatalysts for H_2 evolution when methanol was used as a sacrificial electron donor as reported previously.[23] The TG/DTA data were used to check whether carbonaceous residue remains in mesoporous spheres (Figure S7, Supporting Information) because it influences catalytic performance. The contents of the carbonaceous residues of **NF5** and **NF10a** were calculated from the weight loss started after 200 °C to be around 3.1% and 7.9%, respectively. The weight loss of **NF10b** was only 2.8%, which is the smallest among the spheres. No significant weight loss due to combustion of organic materials was observed for the reference $NiFe_2O_4$. Due to these results, pretreatment for the removal of carbonaceous residue in mesoporous nickel ferrite spheres was performed by photoirradiation (λ > 420 nm) of an aqueous solution (5 mL) containing the nickel ferrite spheres for 2 h under atmospheric conditions before performing H_2 evolution reactions. The evolved gas during the reaction was analyzed by GC. CO_2 evolution accompanied by a trace amount of H_2 evolution was observed for the mesoporous nickel ferrite spheres, indicating that carbonaceous residue was oxidatively decomposed to CO_2 during the photoirradiation. After the pretreatment, H_2 evolution was performed by photoirradiation (λ > 420 nm) of a reaction suspension [methanol/water, 1/4 (v/v)] containing mesoporous nickel ferrite. Figure 6 shows the time courses of H_2 evolution by using mesoporous nickel ferrite spheres or reference $NiFe_2O_4$ prepared by sol−gel combustion (2.0 mg) as photocatalysts. The amount of H_2 evolution with **NF10b** (0.44 μmol) observed after 5 h was larger than those of **NF5** (0.09 μmol), **NF10a** (0.09 μmol), and reference $NiFe_2O_4$ (0.16 μmol). A small amount of CO_2 evolution was also detected from the reaction solutions as a result of methanol oxidation as reported previously.[23,43] Thus, mesoporous nickel ferrite spheres catalyze visible light-driven H_2 evolution efficiently using methanol as a sacrificial electron donor.

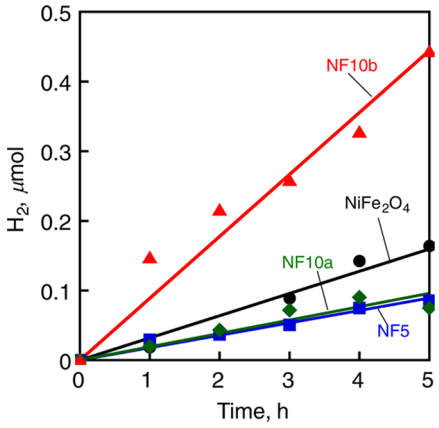

Figure 6. Time courses of H_2 evolution under visible light irradiation (Xe lamp, λ > 420 nm) of a reaction suspension (5.0 mL) [methanol/water, 1/4 (v/v)] containing a photocatalyst (2.0 mg); **NF5** (blue squares), **NF10a** (green diamonds), **NF10b** (red triangles), and reference $NiFe_2O_4$ (black dots).

High crystallinity of semiconductors was reported to improve photocatalytic activity due to an enhancement in electron−hole separation.[44,45] Nickel ferrites with high crystallinity were expected to exhibit improved photocatalytic activity for H_2 evolution.[23] However, the effect of crystallinity on the photocatalytic activity has yet to be clarified, as all nickel ferrite photocatalysts employed in the previous report possessed high crystallinity.[23] In this work, both amorphous and well-crystallized mesoporous nickel ferrites with the same morphology were prepared by the aerosol spray pyrolysis method, providing a good opportunity to evaluate the relationship between catalytic performance and crystallinity. The H_2-evolution rates of the mesoporous nickel ferrites are summarized in Table 1. The highest H_2-evolution rate observed for **NF10b** suggests that high crystallinity of the spinel structure improved the photocatalytic activity of nickel ferrites rather than the surface areas. As compared with **NF5** (0.02 μmol h^{-1}) and **NF10a** (0.02 μmol h^{-1}) bearing low crystallinity of the spinel structure, the higher rate of H_2 evolution was obtained for **NF10b** (0.09 μmol h^{-1}) and reference $NiFe_2O_4$ (0.03 μmol h^{-1}) with high crystallinity. The rate of H_2 evolution with **NF10b** was larger than that of reference $NiFe_2O_4$ because of the higher surface area. Thus, comparison of photocatalytic activity among mesoporous nickel ferrites clarifies that the photocatalytic activity for H_2 evolution depends on both primarily crystallinity and then surface areas.

To examine the photoactive wavelength of nickel ferrites, H_2 evolution with **NF10b** was examined by irradiation of monochromatic light (500, 650, and 700 nm). The time course of H_2 evolution dependent on wavelength is shown in Figure S8 of the Supporting Information. The correlation between the H_2-evolution rate and the diffuse reflectance UV−vis spectrum of **NF10b** is exhibited in Figure 7, where the H_2-evolution rate declined sharply from the wavelength of 500 nm accompanied by a decrease in absorption of **NF10b**. This result

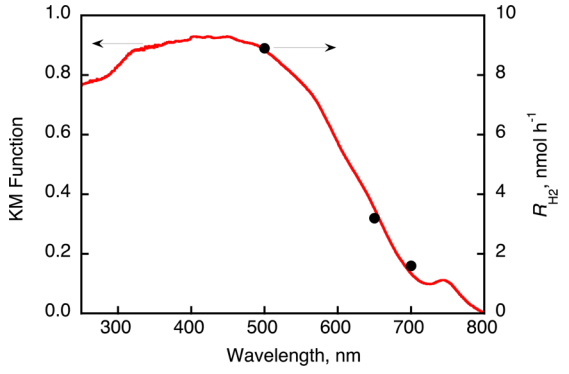

Figure 7. Dependence of H_2-evolution rates (R_{H2}) on the wavelength of monochromatic light irradiation of an aqueous solution (2.0 mL, pH 7.0) containing methanol (0.5 mL) and a photocatalyst of **NF10a** (1.0 mg).

clearly demonstrates that the photoexcitation of **NF10b** contributes to H_2 evolution from water with methanol, and the photoactive wavelength of nickel ferrites is no more than 700 nm, which is consistent with previous reports.[23] An apparent quantum yield was determined to be 7.5×10^{-3}% for the photocatalytic H_2 evolution with **NF10b** by irradiation with monochromatic light ($\lambda = 450 \pm 10$ nm) (see Figure S9 of the Supporting Information for the detail determination method).

As the highest photocatalytic activity was observed for **NF10b**, the robustness of the mesoporous nickel ferrite was also examined. After the first run, **NF10b** was collected by centrifugation and used for further repetitive photoreactions. The time courses of resulting H_2 evolution are shown in Figure 8. The amounts of H_2 evolution for the second and third runs

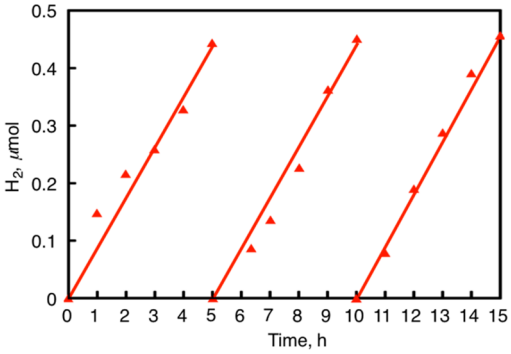

Figure 8. Time courses of H_2 evolution under visible light irradiation (Xe lamp, $\lambda > 420$ nm) of an aqueous solution (4.0 mL, pH 7.0) containing methanol (1.0 mL) and **NF10b** (2.0 mg, red triangles) in 3 repetitive examinations.

after 5 h irradiation (0.43 μmol and 0.46 μmol, respectively) are virtually the same as that of the first run (0.44 μmol). These results clearly indicate that **NF10b** is a highly active and robust photocatalyst for the photocatalytic H_2 evolution.

NF10b was investigated by TEM and powder XRD measurements after the third run photoreaction (Figure S10, Supporting Information). TEM images in Figure S10a of the Supporting Information indicate that both the spherical and mesoporous structures were retained after the H_2 evolution. The powder XRD pattern of **NF10b** after photoreaction exhibits the spinel structure, demonstrating **NF10b** is a durable photocatalyst for the photocatalytic H_2 evolution (Figure S10b, Supporting Information).

CONCLUSIONS

Mesoporous nickel ferrite spheres were prepared by the aerosol spray pyrolysis method and were used as a visible light-driven photocatalyst for H_2 evolution. The surface areas and pore sizes were controlled by altering the ratio between the structure-directing agent and metal oxide precursors during the synthetic process. High crystallinity of the spinel-structured nickel ferrite was obtained by increasing the ramp rates of calcining the product obtained through the aerosol spray pyrolysis method. H_2 evolution was observed by visible light irradiation of the aqueous suspension containing nickel ferrites and methanol. The mesoporous nickel ferrite with high crystallinity and large surface area exhibited the highest photocatalytic activity and robustness for the H_2 evolution among other nickel ferrites. The aerosol spray pyrolysis method to prepare spherical mesoporous metal oxides with high crystallinity employed in this study may have a good potential to be further applied to improve catalytic activity.

ASSOCIATED CONTENT

Supporting Information

Aerosol spray process (Figure S1), TEM images of precursor (Figure S2), SEM images and EDX spectra of **NF5**, **NF10a**, and **NF10b** (Figure S3), powder XRD, SEM images, and EDX spectrum of reference $NiFe_2O_4$ (Figure S4, S5, and S6, respectively), TG/DTA data (Figure S7), time course of H_2 evolution (Figure S8), time course of H_2 evolution with determination of an apparent quantum yield for **NF10b** (Figure S9), and characterizations of **NF10b** after photoreaction (Figure S10). This material is available free of charge via the Internet at http://pubs.acs.org.

AUTHOR INFORMATION

Corresponding Authors

*E-mail: frank.tsung@bc.edu (C.-K.T).
*E-mail: fukuzumi@chem.eng.osaka-u.ac.jp (S.F.).

Notes

The authors declare no competing financial interest.

ACKNOWLEDGMENTS

This work was partially supported by a Grant-in-Aid (24350069 and 25600025) from the MEXT (Japan), an ALCA project from JST, and by NRF/MEST (Korea) through GRL (2010-00353) Programs. D.H. gratefully acknowledges support from JSPS by Grant-in-Aid for JSPS Fellowship for Young Scientists. We acknowledge the Research Centre for Ultra-Precision Science & Technology in Osaka University for TEM measurements.

REFERENCES

(1) Gonçalves, R. H.; Lima, B. H. R.; Leite, E. R. Magnetite colloidal nanocrystals: A facile pathway to prepare mesoporous hematite thin films for photoelectrochemical water splitting. *J. Am. Chem. Soc.* **2011**, *133*, 6012−6019.
(2) Liu, S.; Bai, S.-Q.; Zheng, Y.; Shah, K. W.; Han, M.-Y. Composite metal−oxide nanocatalysts. *ChemCatChem.* **2012**, *4*, 1462−1484.
(3) Taguchi, A.; Schüth, F. Ordered mesoporous materials in catalysis. *Microporous Mesoporous Mater.* **2005**, *77*, 1−45.
(4) Casbeer, E.; Sharma, V. K.; Li, X.-Z. Synthesis and photocatalytic activity of ferrites under visible light: A review. *Sep. Purif. Technol.* **2012**, *87*, 1−14.
(5) Yamada, Y.; Yano, K.; Hong, D.; Fukuzumi, S. $LaCoO_3$ acting as an efficient and robust catalyst for photocatalytic water oxidation with persulfate. *Phys. Chem. Chem. Phys.* **2012**, *14*, 5753−5760.
(6) Hong, D.; Yamada, Y.; Nomura, A.; Fukuzumi, S. Catalytic activity of $NiMnO_3$ for visible light-driven and electrochemical water oxidation. *Phys. Chem. Chem. Phys.* **2013**, *15*, 19125−19128.
(7) Fukuzumi, S.; Hong, D.; Yamada, Y. Bioinspired photocatalytic water reduction and oxidation with earth-abundant metal catalysts. *J. Phys. Chem. Lett.* **2013**, *4*, 3458−3467.
(8) Yang, P.; Zhao, D.; Margolese, D. I.; Chmelka, B. F.; Stucky, G. D. Generalized syntheses of large-pore mesoporous metal oxides with semicrystalline frameworks. *Nature* **1998**, *396*, 152−155.
(9) Ginosar, D. M.; Rollins, H. W.; Petkovic, L. M.; Burch, K. C.; Rush, M. J. High-temperature sulfuric acid decomposition over complex metal oxide catalysts. *Int. J. Hydrogen Energy* **2009**, *34*, 4065−4073.
(10) Banerjee, A. B.; Pai, M. R.; Meena, S. S.; Tripathi, A. K.; Bharadwaj, S. R. Catalytic activities of cobalt, nickel and copper ferrospinels for sulfuric acid decomposition: The high temperature

step in the sulfur based thermochemical water splitting cycles. *Int. J. Hydrogen Energy* **2011**, *36*, 4768−4780.
(11) Santos, P. T. A.; Lira, H. L.; Gama, L.; Argolo, F.; Andrade, H. M. C.; Costa, A. C. F. M. Evaluation of $NiFe_2O_4$ spinel, synthesized by combustion reaction, as a catalyst for selective CO oxidation. *Sci. Forum* **2010**, *660−661*, 771−776.
(12) Gokon, N.; Murayama, H.; Nagasaki, A.; Kodama, T. Thermochemical two-step water splitting cycles by monoclinic ZrO_2-supported $NiFe_2O_4$ and Fe_3O_4 powders and ceramic foam devices. *Sol. Energy* **2009**, *83*, 527−537.
(13) Fresno, F.; Yoshida, T.; Gokon, N.; Fernández-Saavedra, R.; Kodama, T. Comparative study of the activity of nickel ferrites for solar hydrogen production by two-step thermochemical cycles. *Int. J. Hydrogen Energy* **2010**, *35*, 8503−510.
(14) Gokon, N.; Kodama, T.; Imaizumi, N.; Umeda, J.; Seo, T. Ferrite/zirconia-coated foam device prepared by spin coating for solar demonstration of thermochemical water-splitting. *Int. J. Hydrogen Energy* **2011**, *36*, 2014−2028.
(15) Abbaspour, A.; Mirahmadi, E. Electrocatalytic hydrogen evolution reaction on carbon paste electrode modified with Ni ferrite nanoparticles. *Fuel* **2013**, *104*, 575−582.
(16) Maeda, K.; Domen, K. New non-oxide photocatalysts designed for overall water splitting under visible light. *J. Phys. Chem. C* **2007**, *111*, 7851−7861.
(17) Maeda, K.; Teramura, K.; Saito, N.; Inoue, Y.; Kobayashi, H.; Domen, K. Overall water splitting using (oxy)nitride photocatalysts. *Pure Appl. Chem.* **2006**, *78*, 2267−2276.
(18) Osterloh, F. E. Inorganic nanostructures for photoelectrochemical and photocatalytic water splitting. *Chem. Soc. Rev.* **2013**, *42*, 2294−320.
(19) Abe, R.; Shinmei, K.; Koumura, N.; Hara, K.; Ohtani, B. Visible-light-induced water splitting based on two-step photoexcitation between dye-sensitized layered niobate and tungsten oxide photocatalysts in the presence of a triiodide/iodide shuttle redox mediator. *J. Am. Chem. Soc.* **2013**, *135*, 16872−16884.
(20) Navarro, R. M.; Alvarez-Galván, M. C.; Villoria de la Mano, J. A.; Al-Zahrani, S. M.; Fierro, J. L. G. A framework for visible-light water splitting. *Energy Environ. Sci.* **2010**, *3*, 1865−1882.
(21) Kudo, A.; Miseki, Y. Heterogeneous photocatalyst materials for water splitting. *Chem. Soc. Rev.* **2009**, *38*, 253−278.
(22) Chen, X.; Shen, S.; Guo, L.; Mao, S. S. Semiconductor-based photocatalytic hydrogen generation. *Chem. Rev.* **2010**, *110*, 6503−6570.
(23) Peng, T.; Zhang, X.; Lv, H.; Zan, L. Preparation of $NiFe_2O_4$ nanoparticles and its visible-light-driven photoactivity for hydrogen production. *Catal. Commun.* **2012**, *28*, 116−119.
(24) Xu, S.; Shangguan, W.; Yuan, J.; Chen, M. Shi, Preparations and photocatalytic properties of magnetically separable nitrogen-doped TiO_2 supported on nickel ferrite. *Appl. Catal., B* **2007**, *71*, 177−184.
(25) Hong, D.; Yamada, Y.; Nagatomi, T.; Takai, Y.; Fukuzumi, S. Catalysis of nickel ferrite for photocatalytic water oxidation using $[Ru(bpy)_3]^{2+}$ and $S_2O_8^{2-}$. *J. Am. Chem. Soc.* **2012**, *134*, 19572−19575.
(26) Bao, N.; Shen, L.; Wang, Y.; Padhan, P.; Gupta, A. A facile thermolysis route to monodisperse ferrite nanocrystals. *J. Am. Chem. Soc.* **2007**, *129*, 12374−12375.
(27) Kuai, L.; Geng, J.; Chen, C.; Kan, E.; Liu, Y.; Wang, Q.; Geng, B. A reliable aerosol-spray-assisted approach to produce and optimize amorphous metal oxide catalysts for electrochemical water splitting. *Angew. Chem., Int. Ed.* **2014**, *53*, 7547−7551.
(28) Cheng, Y.; Zheng, Y.; Wang, Y.; Bao, F.; Qin, Y. Synthesis and magnetic properties of nickel ferrite nano-octahedra. *J. Solid State Chem.* **2005**, *178*, 2394−2397.
(29) Yáñez-Vilar, S.; Sánchez-Andújar, M.; Gómez-Aguirre, C.; Mira, J.; Señarís-Rodríguez, M. A.; Castro-García, S. A simple solvothermal synthesis of MFe_2O_4 (M=Mn, Co and Ni) nanoparticles. *J. Solid State Chem.* **2009**, *182*, 2685−2690.
(30) Larumbe, S.; Pérez-Landazábal, J. I.; Pastor, J. M.; Gómez-Polo, C. Sol-gel $NiFe_2O_4$ nanoparticles: Effect of the silica coating. *J. Appl. Phys.* **2012**, *111*, 103911.
(31) Deng, H.; Chen, H.; Li, H. Synthesis of crystal MFe_2O_4 (M=Mg, Cu, Ni) microspheres. *Mater. Mater. Chem. Phys.* **2007**, *101*, 509−513.
(32) Gao, Z.; Cui, F.; Zeng, S.; Guo, L.; Shi, J. A high surface area superparamagnetic mesoporous spinel ferrite synthesized by a template-free approach and its adsorptive property. *Microporous Mesoporous Mater.* **2010**, *132*, 188−195.
(33) Areva, S.; Boissiere, C.; Grosso, D.; Asakawa, T.; Sanchez, C.; Linden, M. One-pot aerosol synthesis of ordered hierarchical mesoporous core-shell silica nanoparticles. *Chem. Commun.* **2004**, 1630−1631.
(34) Boissiere, C.; Grosso, D.; Chaumonnot, A.; Nicole, L.; Sanchez, C. Aerosol Route to Functional Nanostructured Inorganic and Hybrid Porous Materials. *Adv. Mater.* **2011**, *23*, 599−623.
(35) Tsung, C.-K.; Fan, J.; Zheng, N.; Shi, Q.; Forman, A. J.; Wang, J.; Stucky, G. D. A general route to diverse mesoporous metal oxide submicrospheres with highly crystalline frameworks. *Angew. Chem., Int. Ed.* **2008**, *47*, 8682−8686.
(36) Ostomel, T. A.; Shi, Q.; Tsung, C.-K.; Liang, H.; Stucky, G. D. Spherical bioactive glass with enhanced rates of hydroxyapatite deposition and hemostatic activity. *Small* **2006**, *2*, 1261−1265.
(37) Li, L.; Tsung, C.-K.; Yang, Z.; Stucky, G. D.; Sun, L. D.; Wang, J. F.; Yan, C. H. Rare-earth-doped nanocrystalline titania microspheres emitting luminescence via energy transfer. *Adv. Mater.* **2008**, *20*, 903−908.
(38) Lu, Y.; Fan, H.; Stump, A.; Ward, T. L.; Rieker, T.; Brinker, C. J. Aerosol-assisted self-assembly of mesostructured spherical nanoparticles. *Nature* **1999**, *398*, 223−226.
(39) Mann, A. K. P.; Skrabalak, S. E. Synthesis of single-crystalline nanoplates by spray pyrolysis: A metathesis route to Bi_2WO_6. *Chem. Mater.* **2011**, *23*, 1017−1022.
(40) Sing, K. S. W.; Everett, D. H.; Haul, R. A. W; Moscou, L.; Pierotti, R. A.; Rouquérol, J.; Siemieniewska, T. Reporting physisorption data for gas/solid systems with special reference to the determination of surface area and porosity. *Pure Appl. Chem.* **1985**, *57*, 603−619.
(41) Markus, M.; Günter, R. Electronic structure and optical band gap determination of $NiFe_2O_4$. *J. Phys.: Condens. Matter* **2014**, *26*, 115503.
(42) Sun, Q.-C.; Sims, H.; Mazumdar, D.; Ma, J. X.; Holinsworth, B. S.; O'Neal, K. R.; Kim, G.; Butler, W. H.; Gupta, A.; Musfeldt, J. L. Optical band gap hierarchy in a magnetic oxide: Electronic structure of $NiFe_2O_4$. *Phys. Rev. B* **2012**, *86*, 205106.
(43) Lv, H.; Ma, L.; Zeng, P.; Ke, D.; Peng, T. Synthesis of floriated $ZnFe_2O_4$ with porous nanorod structures and its photocatalytic hydrogen production under visible light. *J. Mater. Chem.* **2010**, *20*, 3665−3672.
(44) Shankar, K.; Basham, J. I.; Allam, N. K.; Varghese, O. K.; Mor, G. K.; Feng, X.; Paulose, M.; Seabold, J. A.; Choi, K.-S.; Grimes, C. A. Recent advances in the use of TiO_2 nanotube and nanowire arrays for oxidative photoelectrochemistry. *J. Phys. Chem. C* **2009**, *113*, 6327−6359.
(45) Lubberhuizen, W. H.; Vanmaekelbergh, D.; Van Faassen, E. Recombination of photogenerated charge carriers in nanoporous gallium phosphide. *J. Porous Mater.* **2000**, *7*, 147−152.